

# Study on the Mechanism of Black Phosphorus Nanosheets Loading $\text{Sr}^{2+}$ Used in Photothermal Antibacterial Treatment

Gaoqiang Ma<sup>1,\*</sup>, Binyang Li<sup>1,\*</sup>, Jiayong Diao<sup>1</sup>, Yongzhi Zhang<sup>1</sup>, Bing Zhang<sup>1</sup>, Dongni Wu<sup>1</sup>, Houda Gui<sup>1</sup>, Junhao Zhong<sup>1</sup>, Hongguang Zhu<sup>2</sup>, Dongjiao Zhang<sup>1</sup>

<sup>1</sup>Department of Implantology, School and Hospital of Stomatology, Cheeloo College of Medicine, Shandong University & Shandong Key Laboratory of Oral Tissue Regeneration & Shandong Engineering Research Center of Dental Materials and Oral Tissue Regeneration & Shandong Provincial Clinical Research Center for Oral Diseases, Jinan, 250012, People's Republic of China; <sup>2</sup>Department of Stomatology, Weifang People's Hospital, Weifang, 261000, People's Republic of China

\*These authors contributed equally to this work

Correspondence: Dongjiao Zhang; Hongguang Zhu, Email djzhang1109@sdu.edu.cn; zhuhongguang9025@126.com

**Purpose:** Bacterial infections seriously affect the health of patients and their incidence is very high. Photothermal therapy has shown promising prospects in the treatment of bacterial infections as it can effectively kill bacteria and reduce inflammation. Black phosphorus (BP) is an emerging nanoparticle that can generate heat under the action of near-infrared light, it can safely and effectively kill bacteria through photothermal therapy. In this experiment, black phosphorus was used as a photothermal agent to kill bacteria and strontium ions were loaded onto BP to enhance its stability and antibacterial performance.

**Methods:** BP was obtained by liquid phase exfoliation and  $\text{Sr}^{2+}$  was loaded onto the surface of BP by electrostatic interaction.

**Results:** BP-Sr was synthesized via electrostatic interactions and characterized using various techniques. The cytocompatibility of BP-Sr was evaluated by CCK8 assay and live/dead staining which showed no significant cytotoxicity with a concentration not exceed 50  $\mu\text{g}/\text{mL}$ . Meanwhile, the antibacterial effects showed 99% of bacteria died after 10 min under the action of a 2  $\text{W}/\text{cm}^2$  laser and the structure of bacteria was destroyed. Finally, the transcriptomic results suggest that bacteria death may be related to membrane destruction, metabolic disorders, and transport damage. HE staining and Gram staining also showed that inflammation was significantly alleviated after laser treatment.

**Conclusion:** These findings propose a great solution for bacterial infection and also enrich the theoretical framework supporting the application of BP-Sr in the field of antibiosis.

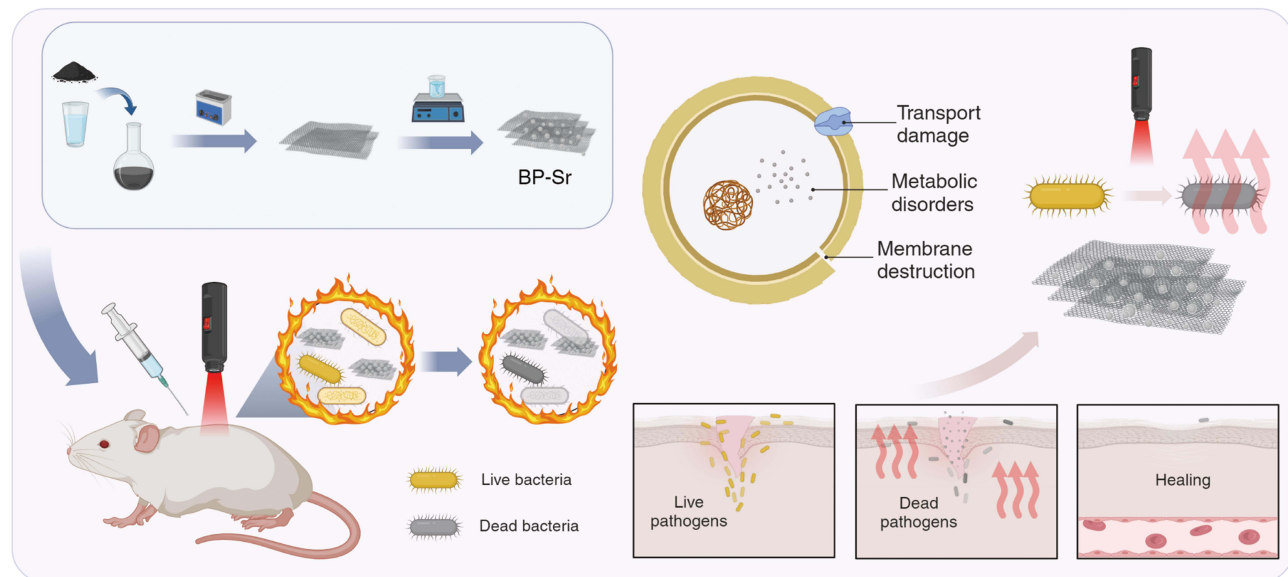
**Keywords:** antibacterial, photothermal therapy, BP-Sr nanosheets, infectious wound

## Introduction

Bacterial infection refers to the invasion and colonization of bacteria leading to local inflammation. Bacterial diseases pose a serious threat to public health. The effective killing of bacteria is crucial for anti-infection treatment and traditional treatment methods mainly include debridement and antibiotic therapy.<sup>1</sup> However, surgical debridement can expand the wound and damage patients, and antibiotic treatment can easily lead to bacterial resistance. Meanwhile, the rate of development of new antibiotics is very slow while bacterial resistance is rapidly increasing. The World Health Organization predicts that the 21st century may be the beginning of the post-antibiotic era, and it is expected that the number of deaths caused by drug-resistant bacteria will increase to millions by 2050.<sup>2</sup>

Photothermal therapy (PTT) is widely studied as an emerging antibacterial therapy. Nanomaterials used for PTT can convert light energy into thermal energy under near-infrared light (NIR) irradiation. On the one hand, it can accelerate tissue healing by promoting vascular regeneration, on the other hand, it can induce bacterial death through protein inactivation, DNA damage and membrane destruction.<sup>3,4</sup> Nanoparticles such as black phosphorus nanosheets,<sup>5</sup>

## Graphical Abstract



phthalocyanine,<sup>6</sup> gold nanorods,<sup>7</sup> and cuttlefish ink nanoparticles<sup>8</sup> have excellent photothermal conversion ability and they could kill bacteria through PTT. Among these, black phosphorus nanosheets exhibit considerable bioactivity and excellent biocompatibility. When exposed to oxygen and water, it can quickly degrade into phosphate, avoiding toxicity or side effects.<sup>9</sup> In addition, it has a large surface area that can be used for drug delivery.<sup>10</sup>

In 2014, black phosphorus nanosheets (BP) were first peeled off and were widely used in the fields of material science and biomedicine.<sup>11</sup> BP is a two-dimensional nanosheet with negative charges on its surface and many excellent properties. BP can produce thermal energy and reactive oxygen species (ROS) within bacteria via photodynamic effects in aerobic environments to exert antibacterial effects without causing bacterial resistance.<sup>12</sup>

However, BP is prone to oxidation reactions in aerobic environments, which affects its photothermal conversion efficiency and limits its role in PTT.<sup>13,14</sup> From a structural perspective, BP has a puckered honeycomb structure, in which phosphorus atoms are bonded to three neighboring phosphorus atoms while exposing a lone pair of electrons.<sup>15</sup> It has been shown that the lone-pair electrons on the surface can be occupied by metal complexes with strong electron-withdrawing capability to retard the natural degradation of BP and introduce extra features.<sup>16,17</sup> Whereas, the combination of BP and metal ions reduces the negative charge of BP, which is conducive to their adhesion to bacteria with a negative surface charge to enhance the sensitivity of bacteria to PTT.<sup>18</sup>

Strontium exists in the human body as  $\text{Sr}^{2+}$  and 99%  $\text{Sr}^{2+}$  present in hard tissues such as bones, making it an essential element of the human body.<sup>19,20</sup> Research shows that  $\text{Sr}^{2+}$  might promote the anabolic effect of osteoblasts and could be used for bone tissue regeneration,<sup>21,22</sup> meanwhile it also has active effects in angiogenesis, anti-inflammatory, antibacterial and other aspects.<sup>23,24</sup> Therefore,  $\text{Sr}^{2+}$  was loaded onto the BP through electrostatic interaction in this experiment, it can weaken the negative charge on the surface of BP which could promote its contact with bacteria and enhance its antibacterial performance.  $\text{Sr}^{2+}$  on the surface of BP can also reduce the loss of phosphorus atoms to enhance its stability and introduce additional biological functions.

This study aimed to obtain BP by liquid-phase exfoliation and load  $\text{Sr}^{2+}$  onto the surface of BP to enhance its bioactivity, stability and antibacterial performance in the treatment of bacterial infections. Transcriptome analysis showed that elevated temperatures can disrupt bacterial defense genes, affecting their normal cellular function and material metabolism.<sup>25</sup> To further explore the mechanism underlying bacterial death under the action of BP-Sr and NIR,

transcriptomic testing was used to investigate the genes in the bacteria at the overall level. Finally, the bacteria-infected full-thickness skin defect model was used to verify the antibacterial performance in Rats.

## Materials and Methods

### Materials Preparation

N-Methylpyrrolidone (NMP) and strontium chloride ( $\text{SrCl}_2$ ) were purchased from MECKLE, BP was purchased from Zhongke Experimental Materials (China), Calcein-AM/PI (Beijing Solarbio Science & Technology Co., Ltd.), Cell-Check™ Viability/Cytotoxicity Kit for Bacteria Cells (ABP Biosciences, China), Cell Counting Kit-8 (Solarbio, China), HE staining kit (Beijing Solarbio Science & Technology Co., Ltd.), and Gram staining kit (Beijing Solarbio Science & Technology Co., Ltd).

### Synthesis of BP-Sr

First, 50 mg BP was thoroughly ground into powders in a mortar and then transferred to a volumetric flask containing 50 mL of NMP solution. Finally, the volumetric flask was sealed. All processes were carried out in an anaerobic environment to protect BP from oxidation. The volumetric flask was placed in an ultrasonic cleaner (300 W, 40 kHz). As the ultrasonic process continued, the BP powder steadily exfoliated into nanosheets. After 10 h, the dispersion was subjected to gradient centrifugation from 4000 to 10,000 rpm (at intervals of 20 min) to remove the residual unexfoliated BP and thicker BP nanosheets. The acquired dispersion was washed with absolute alcohol by centrifugation at 12,000 rpm to remove residual NMP. Finally, the BP nanosheets and sufficient  $\text{SrCl}_2$  were putted into a brown bottle with deionized water, after 5 hours of anaerobic stirring, the solution was subjected to centrifugation (12000 rpm) for 20 min, then, the precipitate was washed and stored in the anaerobic environment.

### Characterization of BP-Sr

The morphology of BP-Sr was observed using scanning electron microscope (SEM, FEI-Quanta 250 FEG, USA). Elemental mapping images were recorded by Energy Dispersive Spectrometer (EDS) equipped in the SEM. The zeta potential of the nanomaterials was measured using a Zeta-sizer Nano ZS90 analyzer (Malvern Instruments Ltd., UK). Ultraviolet-visible (UV-vis) spectra were measured on a PerkinElmer Lambda-35 UV-vis spectrometer.

### In vitro Photothermal Properties

The in vitro photothermal properties of the nanomaterials were investigated in phosphate buffer saline (PBS) using a continuous fiber-coupled semiconductor diode laser (VCL-808 nm; BLUEPRINT, China). Temperature was monitored using a Testo 872 infrared thermal imager.

### The Degradation of BP-Sr

BP-Sr and BP were separately dispersed in deionized water to observe their degradation in vitro. The different solutions were photographed and analyzed using UV-vis spectrophotometry after a month. The concentration of  $\text{PO}_4^{3-}$  was determined using a Malachite Green Phosphate Detection Kit (Beyotime) at a set time.

### Cytotoxicity Testing

Human skin fibroblasts (HSF) were purchased from the iCell Bioscience Inc (Shanghai, China). HSF were seeded into 96-well plates and 24-well plates and incubated at 37 °C, 5%  $\text{CO}_2$  for one day. A cell culture medium containing BP or BP-Sr was used in the experimental group. Then the cells were incubated in a cell incubator. After that, all the medium was aspirated, and each well of the 96-well plates was washed three times with PBS. CCK8 solution was added and the plate was incubated in the cell incubator for 2 h. Finally, the plates were placed in a microplate reader (Thermo Fisher Scientific, USA) to measure the absorbance at 450 nm. Calcein-AM/PI was used for fluorescence staining. After staining for 15 min, the samples were rinsed with PBS and the cells were observed under a fluorescence microscope (Olympus, Japan).

## Antibacterial Performance Testing

The antibacterial effects of BP-Sr on *Staphylococcus aureus* (*S. aureus*, Gram-positive bacteria) and *Escherichia coli* (*E. coli*, Gram-negative bacteria) were evaluated by plate coating method. A single colony of *S. aureus* was dipped with a sterile cotton swab and putted into 1 mL PBS. After being mixed evenly, the concentration of the bacterial solution was adjusted until OD = 0.257 at 600 nm ( $10^8$  CFU/mL), and then was diluted into  $10^4$  CFU/mL. The bacterial suspension was incubated with PBS, BP (50  $\mu$ g/mL) or BP-Sr (50  $\mu$ g/mL) in 96-well plates. NIR irradiation was then performed for 10 min. The bacterial suspension was then plated on LB agar plates and counted. Some bacteria were collected by centrifugation, resuspended in Glutaraldehyde 4% (Beijing Solarbio Science & Technology Co., Ltd.), then the bacteria were fixed on a circular glass sheet for 12 h. Afterwards, the gradient elution was performed for the bacteria with 25%, 50%, 75%, 80%, 90%, and 100% ethanol. Finally, the morphology of the bacteria was observed using SEM. For the live/dead assay, the bacterial precipitate was suspended in 100  $\mu$ L staining solution, and an inverted fluorescence microscope (IX53, Olympus) was used to observe the state of the bacteria.

## Investigation of Antibacterial Mechanism

The ONPG Assay Kit (Beyotime, China), BCA Protein Assay Kit (Beijing Solarbio Science & Technology Co., Ltd.) and AKP Assay Kit (Nanjing Jiancheng, China) were used to detect the membrane destruction. The bacteria of different groups were collected and mixed with ONPG, BCA or AKP working reagent, and the optical density (OD) of the mixture was measured by a spectrophotometer at the corresponding wavelength after setting interval.

## PCR

Total RNA was extracted from the bacteria using Trizol reagent and reverse transcription was performed to obtain cDNA. Real-time PCR analysis was conducted using specific primers for the target genes with 2  $\times$  SYBR Green qPCR Mix (containing ROX) on a LightCycler 480 instrument. 16S rRNA was used as an internal reference and relative mRNA expression levels were quantified. All quantitative results are reported as mean  $\pm$  standard deviation (SD) obtained from at least three independent studies. The statistical differences were calculated using a two-tailed Student's *t*-test. Statistical differences were defined as \*  $p < 0.05$ , \*\*  $p < 0.01$ , \*\*\*  $p < 0.001$ , and \*\*\*\*  $p < 0.0001$ .

## Antibacterial Performance in vivo

Male Wistar rats (250–300 g, 6–8 weeks age) were used for this study. Rats were randomly divided into six groups: PBS, PBS + NIR, BP, BP + NIR, BP-Sr, and BP-Sr + NIR. Full-thickness skin round wounds with a 10 mm diameter were created by needle biopsy, and 50  $\mu$ L bacterial solution (*S. aureus*,  $10^8$  CFU/mL) was added to the wound. For the control group, 50  $\mu$ L PBS was added to the wounds. In the experimental groups, 50  $\mu$ L of BP (50  $\mu$ g/mL) or BP-Sr (50  $\mu$ g/mL) was applied to wounds. Thermal images were obtained by a Testo 872 infrared thermal imager under NIR irradiation. Images of wounds were taken at 1, 3, and 5 days, and Samples were collected on the sixth day to evaluate wound inflammation. After collection, samples were embedded in paraffin and sectioned into slices. Some slices were stained with hematoxylin and eosin (HE) and photographed using a microscope (IX53, Olympus). Others were stained with Gram stain to evaluate bacteria.

## Results and Discussion

### Characterization of BP-Sr

The morphology of BP-Sr was observed by SEM. As shown in [Figure 1A–D](#), both BP and BP-Sr have a thin-layer transparent structure with a size of 1  $\mu$ m and many protrusions occur on the surface of BP-Sr, which may be composed of Sr. In addition, the elemental distribution of BP-Sr was examined ([Figure 1E](#) and [F](#)). According to the elemental maps, the distribution of Sr was homogeneous. The zeta potential of BP was characterized before and after Sr<sup>2+</sup> loading. As shown in [Figure 1G](#), the zeta potential of BP was  $-33.2$  mV and that of BP-Sr was  $-15$  mV. This is attributed to Sr<sup>2+</sup> loaded onto BP through electrostatic interactions, which subsequently shielded part of the negative charge of BP. These results indicated the successful preparation of BP-Sr. Then, the solutions were

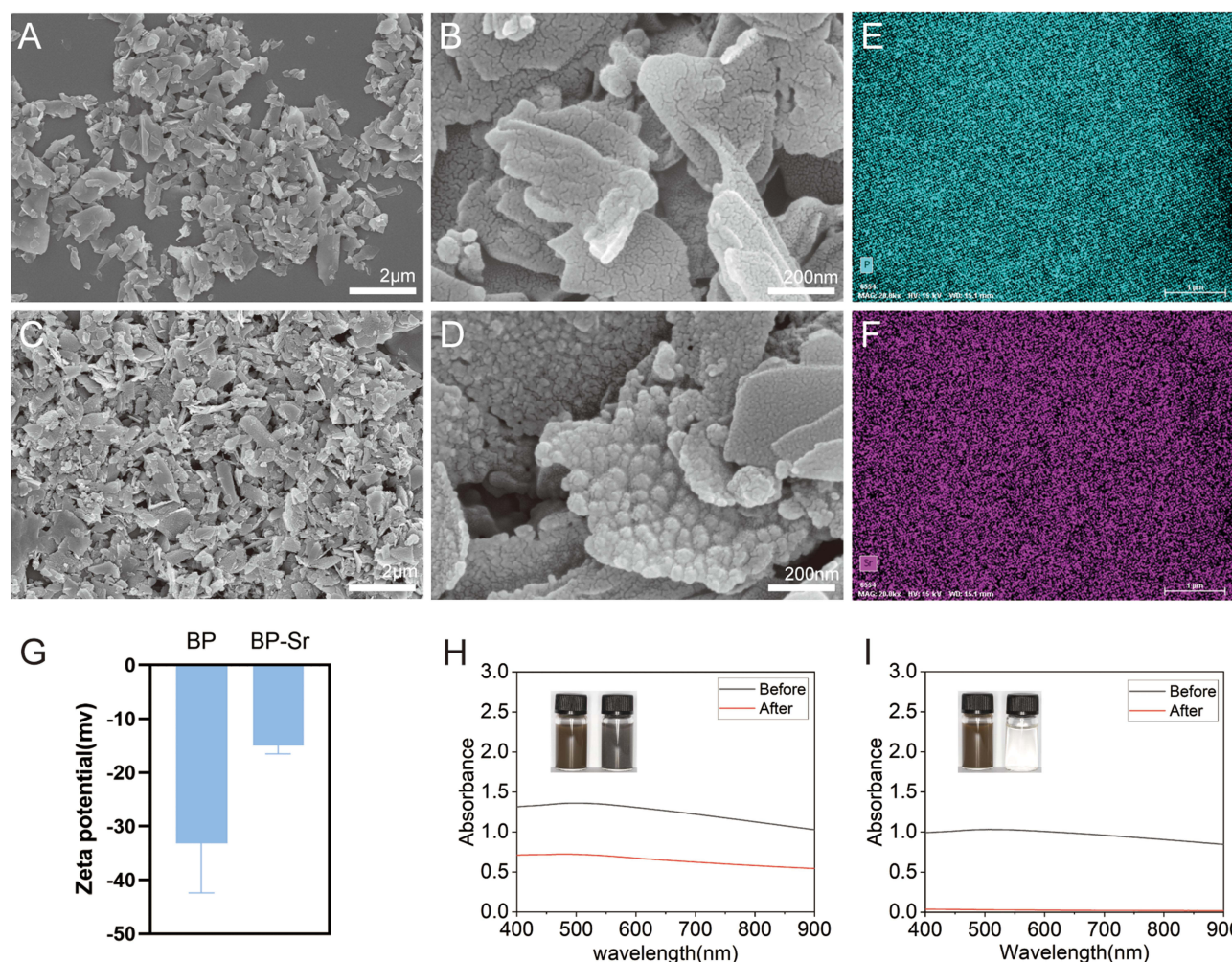


**Figure 1** Characterization of BP-Sr. (A and B) SEM images of BP. (C and D) SEM images of BP-Sr. (E and F) Elemental mapping of BP-Sr. (G) Zeta potential of BP and BP-Sr. (H) Photograph and UV-vis spectrum of BP-Sr. (I) Photograph and UV-vis spectrum of BP.

collected after 1 month to observe degradation. As shown in Figure 1H and I, most of the BP was degraded while BP-Sr remained high, possibly because BP was fully in contact with oxygen in the water, which caused its self-oxidation.<sup>26</sup> Both the images and UV-vis spectra confirmed that the loading of Sr<sup>2+</sup> had a protective effect on BP. The degradation behavior was also studied by monitoring ion release. In addition to degradation, the release of phosphate (PO<sub>4</sub><sup>3-</sup>) into the solution was studied (Figure S1). The release rate of PO<sub>4</sub><sup>3-</sup> from BP was higher than that from BP-Sr which means BP-Sr has better stability.

## In vitro Photothermal Properties

As shown in Figure 2A, the temperatures of BP (50 μg/mL) and BP-Sr (50 μg/mL) suspensions increased with NIR irradiation. As shown in Figure 2B, the temperature of BP-Sr reached 52.5 °C upon NIR irradiation for 10 min, which was higher than that of the control group. This shows that BP-Sr has an excellent photothermal conversion ability. In addition, the photothermal stability of BP-Sr was investigated by circulating intermittent irradiation (lighting for 5 min, cooling for 20 min). As shown in Figure 2C and D, BP-Sr still had a good photothermal conversion ability after four cycles and BP-Sr also had a good performance after one week (Figure 2E). These results indicate that BP-Sr has good photothermal stability.

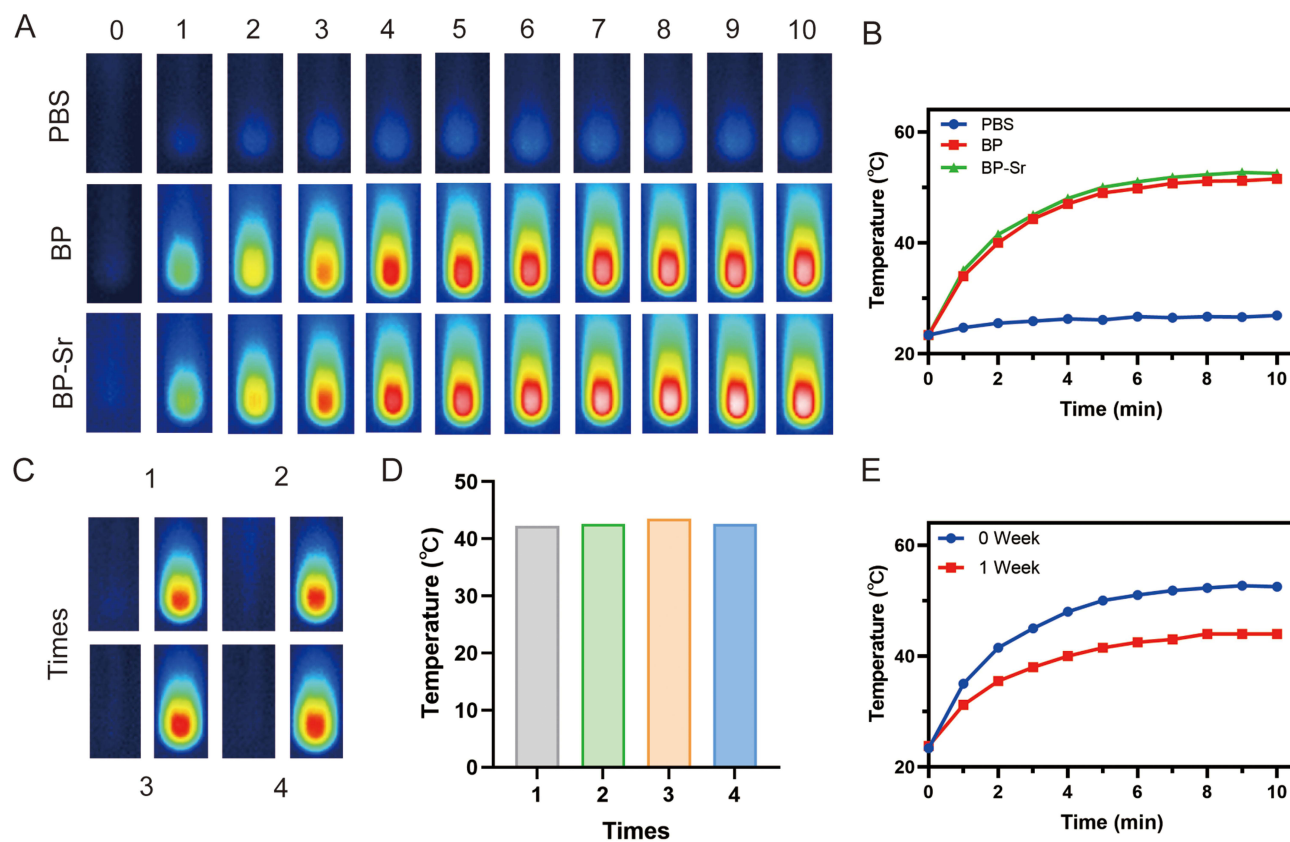


**Figure 2** In Vitro Photothermal Properties. (A and B) Thermal imagery and photothermal heating curves of the BP and BP-Sr upon NIR irradiation (808 nm, 2.0 W cm<sup>2</sup>). (C and D) Cyclic heating profile of BP-Sr for four on/off cycles. (E) Photothermal heating curves of BP-Sr after degradation.

### Cytotoxicity Testing

According to previous reports, when the concentration of BP exceeds 50 μg/mL, it exhibits a certain degree of cytotoxicity.<sup>27</sup> Moreover, the toxicity of BP is also related to the particle size, the larger the particle size, the higher the toxicity.<sup>28</sup> Therefore, the cytotoxicity of BP and BP-Sr was observed in this experiment. CCK8 assay indicated that BP and BP-Sr showed no significant cytotoxicity in HSF with a concentration not exceed 50 μg/mL which is consist with other articles,<sup>10</sup> and the loading of Sr<sup>2+</sup> could also promote cell proliferation. (Figure 3A and S2). Similarly, AM/PI staining showed that BP and BP-Sr did not significantly affect cell viability (Figure 3B).

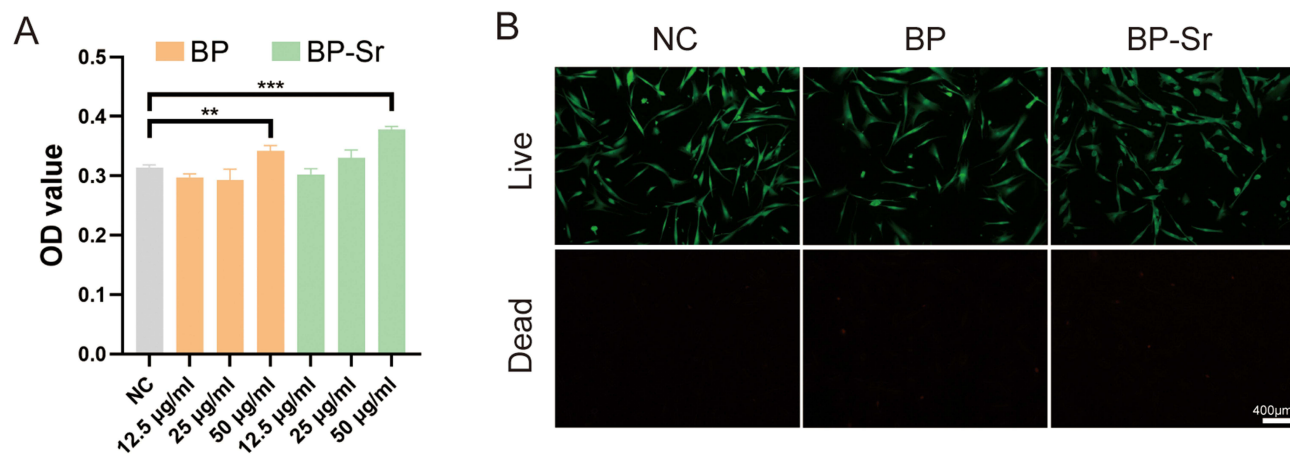


**Figure 3** Cytotoxicity characterization. (A) Viability of HSF measured by CCK8 assay. (B) AM/PI staining of HSF. Data are presented as mean ± SD (\*\*P < 0.01, \*\*\*P < 0.001).

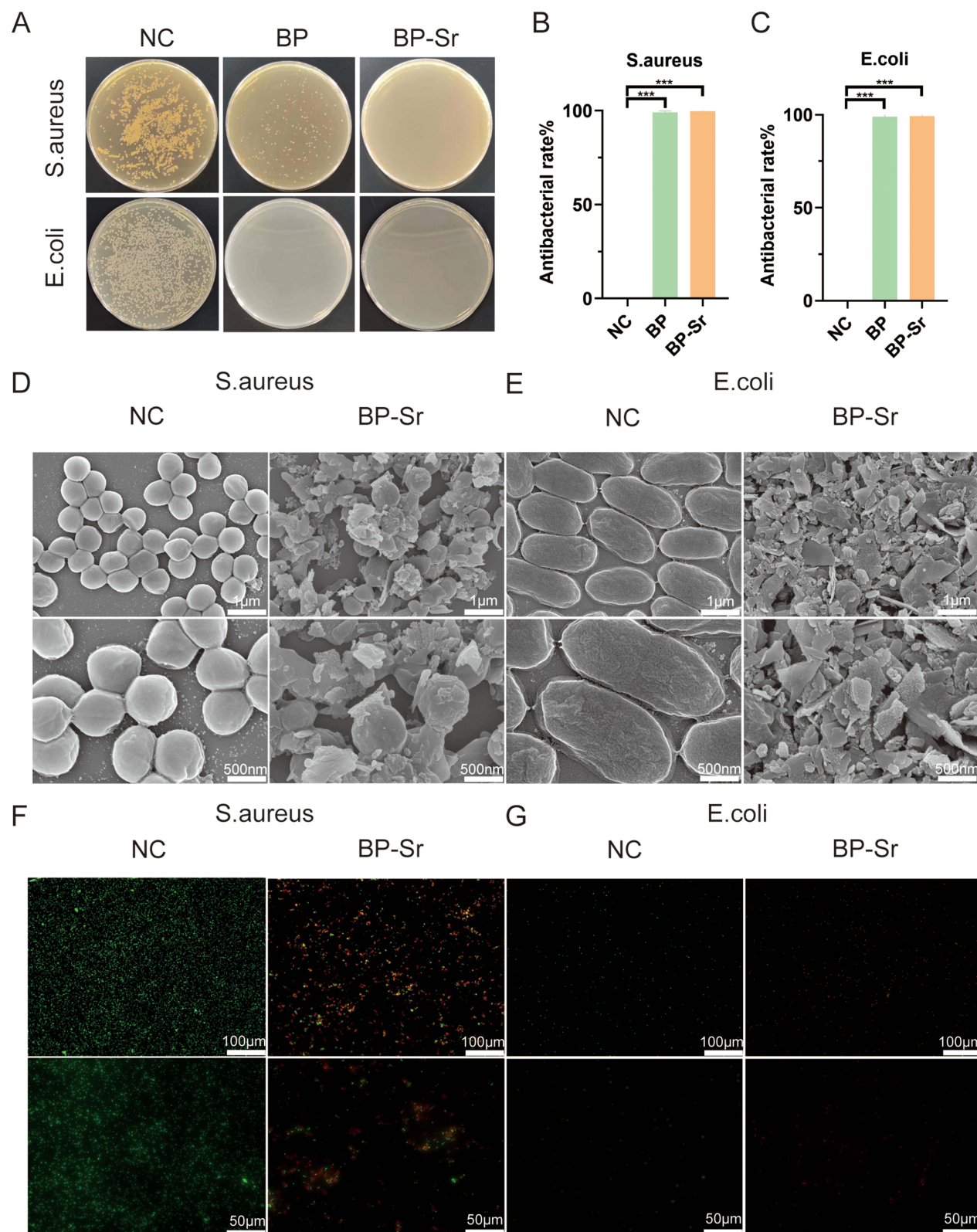


**Figure 4** Antibacterial activity of BP-Sr. (A) Images of agar culture plate bacterial colonies in different groups. (B and C) Antibacterial rate of different groups. (D and E) The SEM images of bacteria. (F and G) Live/dead staining images of bacteria. Data are presented as mean  $\pm$  SD (\*\*P < 0.001).

BP-Sr can release  $\text{PO}_4^{3-}$  and  $\text{Sr}^{2+}$  which have the ability to promote bone regeneration.<sup>29,30</sup> Subsequently, the osteogenic potential of BP-Sr was investigated. The formation of mineralized substances on the surface of BP-Sr was

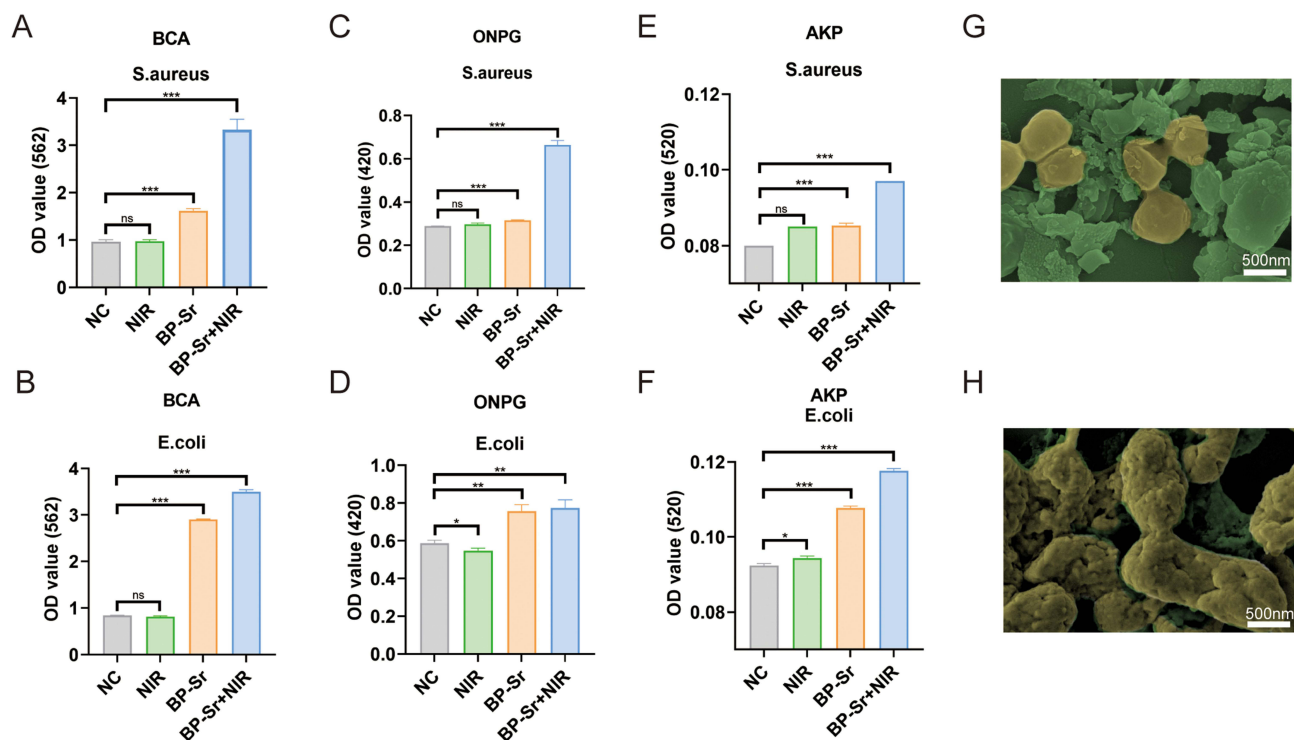


**Figure 5** Antibacterial mechanism of BP-Sr. (A and B) The results of BCA. (C and D) The results of ONPG. (E and F) The results of AKP. (G and H) SEM images of *S. aureus* and *E. coli* after treatment. Data are presented as mean  $\pm$  SD (ns  $P > 0.05$ , \* $P < 0.05$ , \*\* $P < 0.01$ , \*\*\* $P < 0.001$ ).

observed in vitro, and the results of the ALP assay confirmed its osteogenic ability, proving its potential for application in the infection of bone tissues (Figure S3).

## Antibacterial Performance Testing

The results of agar plating of each group after antibacterial treatment are shown in Figure 4A and S4. The control group showed a large number of viable *S. aureus* or *E. coli* colonies. In contrast, the number of colonies in the experimental groups treated with BP + NIR or BP-Sr + NIR decreased to a very low level and the BP-Sr showed a better antibacterial performance. As shown in Figure 4B and C, the bactericidal effects of BP-Sr on *S. aureus* and *E. coli* were as high as 99.5% and 99.8% after a 10 min irradiation indicating its excellent bactericidal ability. The improved antibacterial performance was due to the weakened negative charge on the BP surface which promoted contact with bacteria and the antibacterial potential of  $\text{Sr}^{2+}$ .<sup>18</sup> Bacteria were collected after treatment and observed with SEM. The structure of the control group was complete, but that of the experimental group was destroyed (Figure 4D and E). Live and dead staining was also performed, and it was found that a large number of bacteria in the experimental group died, whereas those in the control group were still alive (Figure 4F and G).

## Antibacterial Mechanism of BP-Sr Based on PTT

Previous studies have shown that increasing temperature enhances the permeability of bacterial membranes, leading to protein leakage.<sup>31</sup> In this experiment, protein leakage was detected to characterize membrane destruction. As shown in Figure 5A and B, the protein concentration in the BP-Sr + NIR group was higher than that in the control group, indicating membrane destruction. The ONPG assay was performed to determine the extent of destruction. As shown in Figure 5C and D, OD405 increased after treatment with BP-Sr + NIR compared to that in the control group. The results of the AKP assay showed a similar pattern (Figure 5E and F), and the morphologies of the different bacteria showed increased destruction (Figure 5G and H). In summary, these results suggest that the antibacterial mechanism of BP-Sr based on PTT is related to destruction of the bacterial membrane.

## Transcriptomic Analysis of *S. aureus*

As shown in [Figure S5](#), the morphology of the colony has undergone significant changes after 6 min NIR which was a more suitable time to prepare bacteria for transcriptomic analysis. Afterwards, differentially expressed genes (DEGs) of *S. aureus* were analyzed by mRNA sequencing (RNA-seq) to study the underlying mechanism of BP-Sr for PTT. As shown in [Figure 6A and B](#), 355 DEGs were identified, including 212 upregulated and 143 downregulated genes ( $|\log_2(\text{fold change})| \geq 0.57$ ,  $P < 0.05$ ).

The 25 downregulated genes with the greatest changes were mainly involved in energy metabolism, riboflavin synthesis and material transport. In [Figure 6C](#), Gene Ontology (GO) enrichment analysis showed that biological processes, such as biological regulation and regulation of cellular processes, were the most enriched GO terms, indicating their significant influence on *S. aureus*. According to the Kyoto Encyclopedia of Genes and Genomes (KEGG) analysis ([Figure 6D](#)), the enrichment of DEGs in membrane transport and signal transduction further confirmed their considerable effect on bacterial membranes. Meanwhile, signaling pathways related to amino acid metabolism, metabolism of cofactors and vitamins and carbohydrate metabolism were significantly altered indicating that the metabolic system of *S. aureus* was affected by BP-Sr based on PTT.

DEGs were then used to create functional protein association networks. The results showed that some proteins have connections in function, and other proteins in the local networks obtained from them are also in line with the relevant

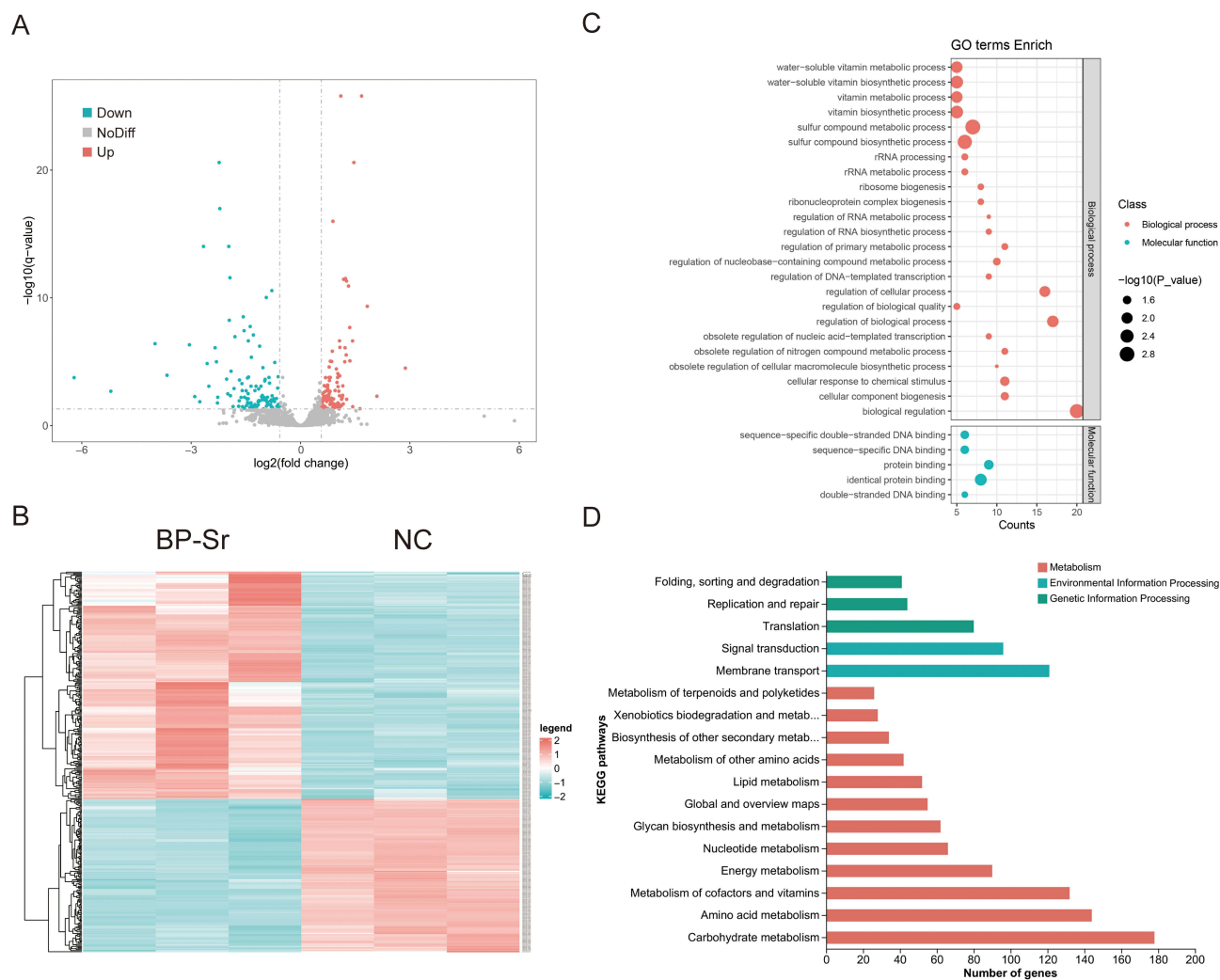


**Figure 6** Changes in the transcriptome of *S. aureus*. **(A)** Volcano plot of DEGs. **(B)** DEGs visualized by heat map analysis. **(C)** GO enriched functional terms of DEGs. **(D)** KEGG of DEGs.

function, further indicating the destruction of riboflavin synthesis, energy metabolism, DNA synthesis, membrane structure, material transport and other functions. The expression levels of the selected DEGs were detected using qRT-PCR. Riboflavin plays a crucial role in bacterial respiration and metabolism, it can help bacteria resist external stimuli. The lack of riboflavin influences the growth of bacteria. As shown in **Figure 7A**, the expression of the related genes (SAOUHSC\_01887, SAOUHSC\_01888 and SAOUHSC\_01889) was significantly downregulated under PTT, indicating a decrease in bacterial resistance.<sup>32</sup> The downregulation of *hisG* and *hisZ*, which are related to energy metabolism, plays an important role in the regulation of microbial growth,<sup>33</sup> indicating a disturbance in energy homeostasis (**Figure 7B**). As

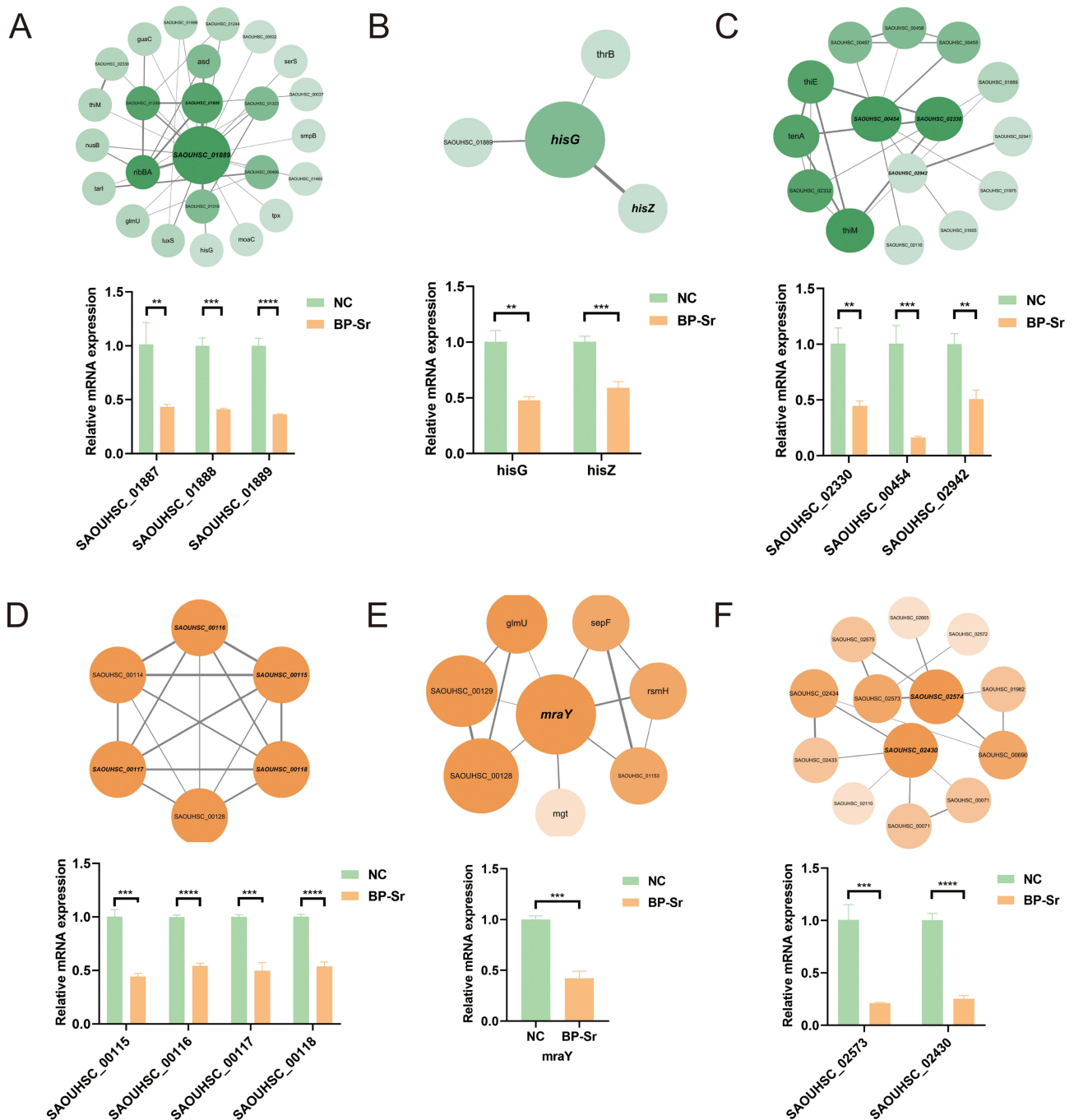


**Figure 7** Functional protein association networks and comparison of the expression profiles of DEGs by qRT-PCR. **(A)** Genes related to riboflavin. **(B)** Genes related to energy metabolism. **(C)** Genes related to DNA. **(D)** Genes related to capsule. **(E)** Genes related to peptidoglycan. **(F)** Genes related to transport. Data are presented as mean  $\pm$  SD (\*\*P < 0.01, \*\*\*P < 0.001, \*\*\*\*P < 0.0001).

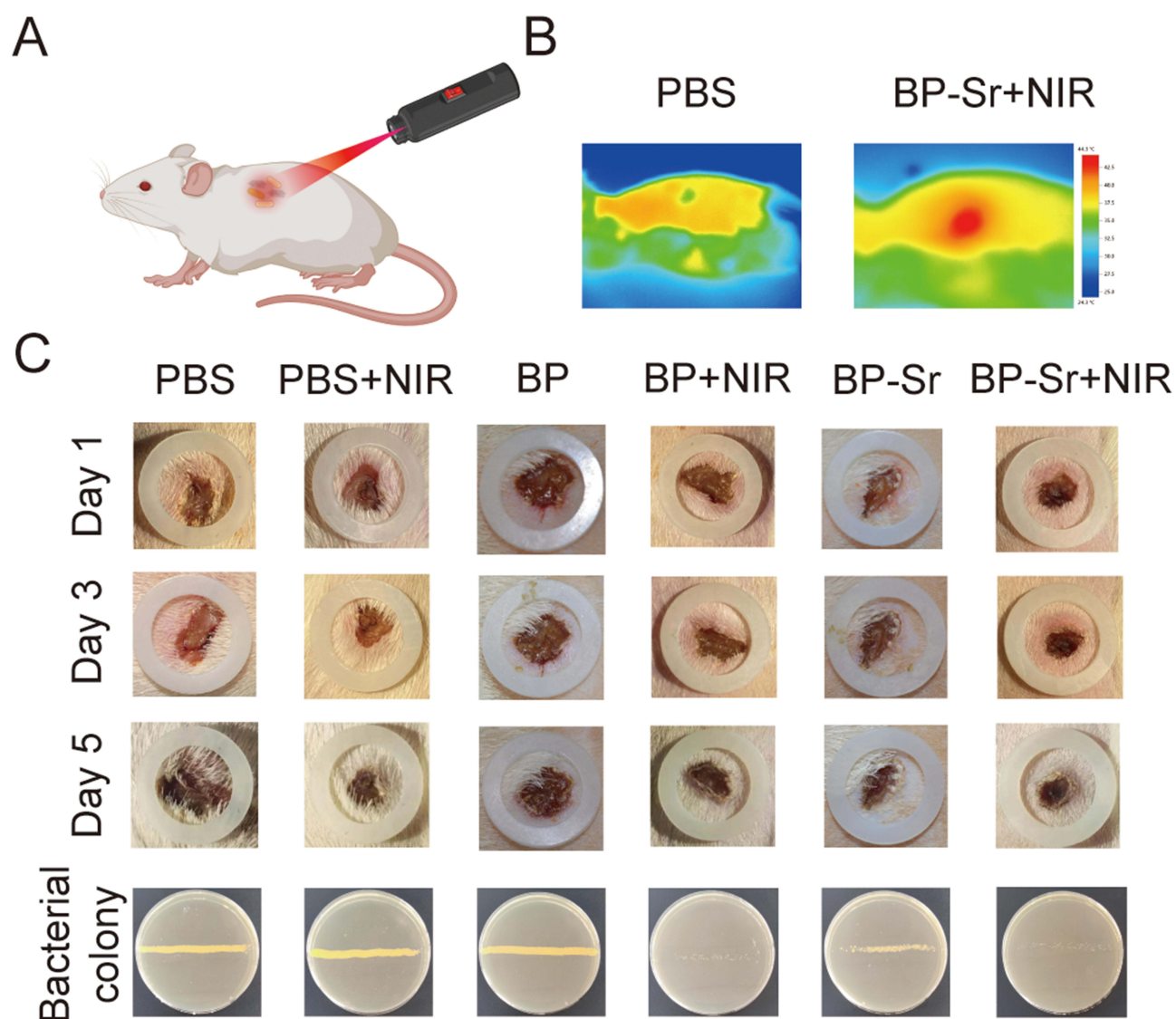


**Figure 8** The antibacterial experiments in vivo. **(A and B)** Thermal images of the BP-Sr in vivo upon NIR irradiation. **(C)** Wound healing of different groups and bacterial colonies on agar plates after cultivation.

shown in [Figure 7C](#), some genes related to DNA replication and repair were downregulated, including SAOUHSC\_02330, SAOUHSC\_00454 and SAOUHSC\_02942. This indicates that bacterial genes related to DNA replication and repair are destroyed, which induces the death under the action of PTT. Leukotoxin is a main pathogenic virulence factor of *S. aureus*,<sup>34</sup> and was significantly downregulated, indicating that the pathogenicity of *S. aureus* had decreased ([Figure S6](#)).

It has been reported that *mraY* participates in the synthesis of peptidoglycan, which is an indispensable component of the cell wall,<sup>35</sup> SAOUHSC\_00115, SAOUHSC\_00116, SAOUHSC\_00117 and SAOUHSC\_00118 participate in the synthesis of capsular polysaccharides, and SAOUHSC\_02430 and SAOUHSC\_2573 are related to material transport on the surface of the cell membrane. Their expression was downregulated implying destruction of the membrane, which was reported to be a significant mechanism of bacterial death under PTT and it is consistent with previous results ([Figure 7D–F](#)). These results further proved that the heat generated by BP-Sr disrupts the homeostasis of *S. aureus*.

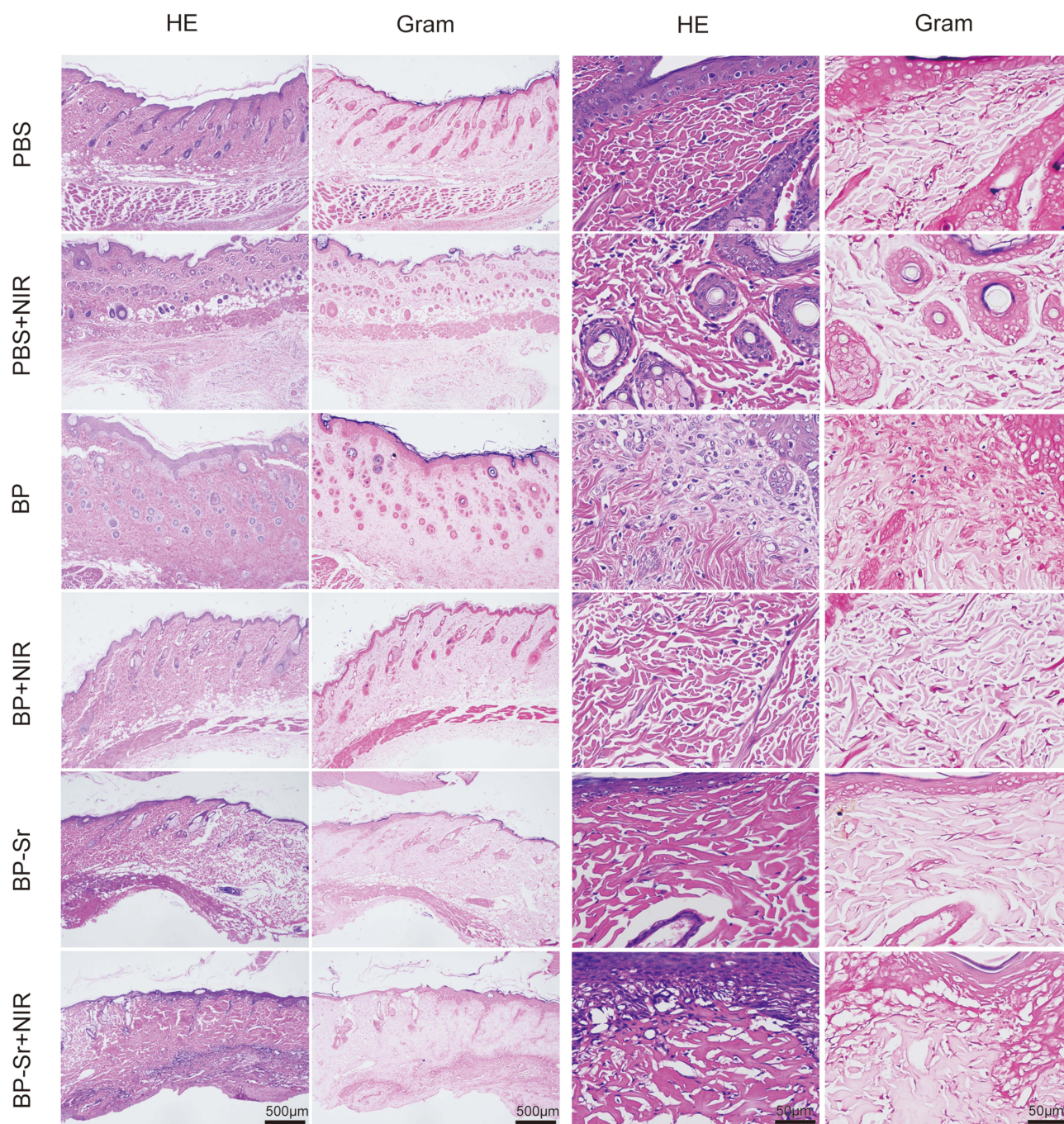


**Figure 9** Histopathological staining. HE staining images showing the degree of infection and Gram staining images revealing the bacteria distribution.

## Antibacterial Performance in Vivo

The antibacterial performance of BP-Sr was evaluated using a bacteria-infected full-thickness skin defect model. As shown in [Figure 8A](#) and [B](#), the temperature of the BP-Sr + NIR group rose to 44.3 °C within 2 min, but the control group did not show significant changes under the same conditions. Bacteria on the wound were collected using cotton swabs and cultured for 12 h. As shown in [Figure 8C](#), bacterial colonies in the BP-Sr + NIR group were smaller, indicating the presence of fewer bacteria. The wound area is also displayed on the 1st, 3rd, and 5th day. On the 5th day, all groups demonstrated wound area contraction to some extent, and the BP-Sr + NIR group demonstrated a smaller wound area than the control group.

To evaluate the degree of infection after treatment, tissues around the wounds were harvested from the different groups and evaluated by histological analysis. As shown in Figure 9, inflammatory cells and bacteria were observed in the tissues of the PBS group owing to serious bacterial infections. In contrast, the inflammatory state was negligible and nearly no bacterial contamination was observed in the tissues of the BP-Sr + NIR group on account of the satisfactory antibacterial performance. Hence, the BP-Sr + NIR group exhibited an excellent antibacterial performance in vivo.

## Conclusion

BP is a photothermal agent used in PTT and is well known for its excellent degradability and photothermal conversion performance. In this experiment, Sr<sup>2+</sup> was loaded onto the surface of BP through electrostatic interactions to improve its stability, antibacterial performance and biological performance. Furthermore, the research on the microstructure and internal antibacterial mechanism has shown that bacterial death is related to structural damage under the intense PTT which could reveal the essence of bacterial death and provides further evidences for the application of BP-Sr in antibiosis. Based on the good antibacterial performance and high biocompatibility, the BP-Sr could be used as an ideal ingredient in tissue engineering to prevent bacterial infection and promote wound healing.

## Acknowledgments

Gaoqiang Ma and Binyang Li contributed equally to this work and are co-first authors for this study. All animal experiments conducted in this study were subjected to thorough review and approval by the Laboratory Animal Ethical and Welfare Committee of Shandong University Cheeloo College of Medicine (NO.24031). The laboratory animals were handled in accordance with the Guidelines for the Care and Use of Laboratory Animals and the Animal Welfare Act in China.

## Funding

This work was supported by the National Natural Science Foundation of China (82071148 and 82201101) and Natural Science Foundation of Shandong Province (ZR2021MH092), and the Construction Engineering Special Fund of Taishan Scholars (grant numbers tsqn202408357).

## Disclosure

The authors declare no competing financial interest.

## References

- Kaminski B, Blochowiak K, Kolomanski K, Sikora M, Karwan S, Chlubek D. Oral and Maxillofacial Infections-A Bacterial and Clinical Cross-Section. *J Clin Med*. 2022;11(10):2731. doi:10.3390/jcm11102731
- Wang Y, Yang Y, Shi Y, Song H, Yu C. Antibiotic-Free Antibacterial Strategies Enabled by Nanomaterials: progress and Perspectives. *Adv Mater*. 2020;32(18):1904106. doi:10.1002/adma.201904106
- Munthe C, Nijssingh N. Cutting red tape to manage public health threats: an ethical dilemma of expediting antibiotic drug innovation. *Bioethics*. 2019;33(7):785–791. doi:10.1111/bioe.12605
- Brown E, Wright G. Antibacterial drug discovery in the resistance era. *Nature*. 2016;529(7586):336–343. doi:10.1038/nature17042
- Wu Y, Liao Q, Wu L, et al. ZnL2-BPs Integrated Bone Scaffold under Sequential Photothermal Mediation: a Win-Win Strategy Delivering Antibacterial Therapy and Fostering Osteogenesis Thereafter. *ACS Nano*. 2021;15(11):17854–17869. doi:10.1021/acsnano.1c06062
- Ouyang A, Zhao D, Wang X, et al. Covalent RGD-graphene-phthalocyanine nanocomposite for fluorescence imaging-guided dual active/passive tumor-targeted combinatorial phototherapy. *J Mater Chem B*. 2022;10(2):306–320. doi:10.1039/D1TB02254G
- Huang S, Hou Y, Tang Z, et al. Near-infrared-II responsive ovalbumin functionalized gold-genipin nanosystem cascading photo-immunotherapy of cancer. *Nanotechnology*. 2024;20:35.
- Xiang Y, Pan Z, Qi X, et al. A cuttlefish ink nanoparticle-reinforced biopolymer hydrogel with robust adhesive and immunomodulatory features for treating oral ulcers in diabetes. *Bioact Mater*. 2024;39:562–581. doi:10.1016/j.bioactmat.2024.04.022
- Huang X, Zhou Y, Woo C, Pan Y, Nie L, Lai P. Multifunctional layered black phosphorene-based nanoplatform for disease diagnosis and treatment: a review. *Front Optoelectron*. 2020;13(4):327–351. doi:10.1007/s12200-020-1084-1
- Zheng H, Li H, Deng H, et al. Near infrared light-responsive and drug-loaded black phosphorus nanosheets for antibacterial applications. *Colloids Surf B Biointerfaces*. 2022;214:112433. doi:10.1016/j.colsurfb.2022.112433
- Xing C, Zhang J, Jing J, et al. Preparations, properties and applications of low-dimensional black phosphorus. *Chem Eng J*. 2019;370:120–135. doi:10.1016/j.cej.2019.03.177
- Liu B, Su Y, Wu S, Shen J. Local photothermal/photodynamic synergistic antibacterial therapy based on two-dimensional BP@CQDs triggered by single NIR light source. *Photodiagnosis Photodyn Ther*. 2022;39:102905. doi:10.1016/j.pdpdt.2022.102905

13. Xie H, Shao J, Ma Y, et al. Biodegradable near-infrared-photoresponsive shape memory implants based on black phosphorus nanofillers. *Biomaterials*. 2018;164:11–21. doi:10.1016/j.biomaterials.2018.02.040
14. Wu J, Mao N, Xie L, Xu H, Zhang J. Identifying the Crystalline Orientation of Black Phosphorus Using Angle-Resolved Polarized Raman Spectroscopy. *Angew Chem Int Ed Engl*. 2015;54(8):2366–2369. doi:10.1002/anie.201410108
15. Rodin A, Carvalho A, Neto A. Strain-Induced Gap Modification in Black Phosphorus. *Phys Rev Lett*. 2014;112(17):176801. doi:10.1103/PhysRevLett.112.176801
16. Zhao Y, Wang H, Huang H, et al. Surface Coordination of Black Phosphorus for Robust Air and Water Stability. *Angew Chem Int Ed Engl*. 2016;55(16):5003–5007. doi:10.1002/anie.201512038
17. Wu L, Wang J, Lu J, et al. Lanthanide-Coordinated Black Phosphorus. *Small*. 2018;14(29):1801405. doi:10.1002/sml.201801405
18. Du J, Cong Y, Wang X, Kang Y, Zhang P, Li L. Green Synthesis of Antimicrobial Peptide-Protected Silver Nanoclusters with Regulated Antibacterial Behavior. *ACS Appl Bio Mater*. 2023;6(9):3919–3926. doi:10.1021/acsabm.3c00646
19. Nightengale B, Brune M, Blizzard S, et al. Strontium chloride Sr 89 for treating pain from metastatic bone disease[J]. *Am J Health Syst Pharm*. 1995;52(20):2189–2195. doi:10.1093/ajhp/52.20.2189
20. Pasqualetti S, Banfi G, Mariotti M. The effects of strontium on skeletal development in zebrafish embryo. *J Trace Elem Med Biol*. 2013;27(4):375–379. doi:10.1016/j.jtemb.2013.06.002
21. Borciani G, Montalbano G, Perut F, Ciapetti G, Baldini N, Vitale-Brovarone C. Osteoblast and osteoclast activity on collagen-based 3D printed scaffolds enriched with strontium-doped bioactive glasses and hydroxyapatite nanorods for bone tissue engineering. *Biomed Mater*. 2024;19(6):065007. doi:10.1088/1748-605X/ad72c3
22. Yu X, Gholipourmalekabadi M, Wang X, Yuan C, Lin K. Three-dimensional bioprinting biphasic multicellular living scaffold facilitates osteochondral defect regeneration. *Interdiscip Mater*. 2024;3:738–756.
23. Liu J, Rawlinson S, Hill R, et al. Strontium-substituted bioactive glasses in vitro osteogenic and antibacterial effects[J]. *Dent Mater*. 2016;32(3):412–422. doi:10.1016/j.dental.2015.12.013
24. Lu W, Zhou C, Ma Y, et al. Improved osseointegration of strontium-modified titanium implants by regulating angiogenesis and macrophage polarization. *Biomater Sci*. 2022;10(9):2198–2214. doi:10.1039/D1BM01488A
25. Jin W, Song P, Wu Y, et al. Biofilm Microenvironment-Mediated MoS<sub>2</sub> Nanoplatfom with Its Photothermal/Photodynamic Synergistic Antibacterial Molecular Mechanism and Wound Healing Study. *ACS Biomater Sci Eng*. 2022;8(10):4274–4288. doi:10.1021/acsbomaterials.2c00856
26. Doganov R, O'Farrell E, Koenig S, et al. Transport properties of pristine few-layer black phosphorus by van der Waals passivation in an inert atmosphere. *Nat Commun*. 2015;6(1):6647. doi:10.1038/ncomms7647
27. Lee H, Park S, Lee S, et al. Black Phosphorus (BP) Nanodots for Potential Biomedical Applications. *Small*. 2016;12(2):214–219. doi:10.1002/sml.201502756
28. Zhang X, Zhang Z, Zhang S, et al. Size Effect on the Cytotoxicity of Layered Black Phosphorus and Underlying Mechanisms. *Small*. 2017;13(32):1210. doi:10.1002/sml.201701210.
29. Xingge Y, Jiang S, Dejian L, Steve GFS, Wang X, Lin K. Osteoimmunomodulatory bioinks for 3D bioprinting achieve complete regeneration of critical-sized bone defects. *Composites Part B*. 2024;273:1359–8368.
30. Li D, Chen K, Duan L, et al. Strontium Ranelate Incorporated Enzyme-Cross-Linked Gelatin Nanoparticle/Silk Fibroin Aerogel for Osteogenesis in OVX-Induced Osteoporosis. *ACS Biomater Sci Eng*. 2019;5(3):1440–1451. doi:10.1021/acsbomaterials.8b01298
31. Xu B, Yu D, Xu C, et al. Study on synergistic mechanism of molybdenum disulfide/sodium carboxymethyl cellulose composite nanofiber mats for photothermal/photodynamic antibacterial treatment. *Int J Biol Macromol*. 2024;266(Pt 1):130838. doi:10.1016/j.ijbiomac.2024.130838
32. Lei J, Xin C, Xiao W, et al. The promise of endogenous and exogenous riboflavin in antiinfection. *Virulence*. 2021;12(1):2314–2326. doi:10.1080/21505594.2021.1963909
33. Lohkamp B, McDermott G, Campbell S, Coggins J, Laphorn A. The structure of Escherichia coli ATP-phosphoribosyltransferase: identification of substrate binding sites and mode of AMP inhibition. *J mol Biol*. 2004;336(1):131–144. doi:10.1016/j.jmb.2003.12.020
34. Nocadello S, Minasov G, Shuvalova L, et al. Crystal structures of the components of the Staphylococcus aureus leukotoxin ED. *Acta Crystallogr D Struct Biol*. 2016;72(Pt 1):113–120. doi:10.1107/S2059798315023207
35. Bouhss A, Mengin-Lecreulx D, Le B, Van H. Topological analysis of the MraY protein catalysing the first membrane step of peptidoglycan synthesis. *Mol Microbiol*. 1999;34(3):576–585. doi:10.1046/j.1365-2958.1999.01623.x

International Journal of Nanomedicine

Publish your work in this journal

The International Journal of Nanomedicine is an international, peer-reviewed journal focusing on the application of nanotechnology in diagnostics, therapeutics, and drug delivery systems throughout the biomedical field. This journal is indexed on PubMed Central, MedLine, CAS, SciSearch®, Current Contents®/Clinical Medicine, Journal Citation Reports/Science Edition, EMBase, Scopus and the Elsevier Bibliographic databases. The manuscript management system is completely online and includes a very quick and fair peer-review system, which is all easy to use. Visit <http://www.dovepress.com/testimonials.php> to read real quotes from published authors.

Submit your manuscript here: <https://www.dovepress.com/international-journal-of-nanomedicine-journal>

**Dovepress**  
Taylor & Francis Group